


Accurate photonic temporal mode analysis with reduced resourcesO. Morin , S. Langenfeld, M. Körber, and G. Rempe*Max Planck Institut für Quantenoptik, Hans-Kopfermann-Strasse 1, D-85748 Garching, Germany*

(Received 29 May 2019; revised manuscript received 16 November 2019; published 2 January 2020)

The knowledge and thus characterization of the temporal modes of quantum light fields is important in many areas of quantum physics ranging from experimental setup diagnosis to fundamental-physics investigations. Recent results showed how the autocorrelation function computed from continuous-wave homodyne measurements can be a powerful way to access the temporal mode structure. Here, we push forward this method by providing a deeper understanding and by showing how to extract the amplitude and phase of the temporal mode function with reduced experimental resources. Moreover, a quantitative analysis allows us to identify a regime of parameters where the method provides a trustworthy reconstruction, which we illustrate experimentally.

DOI: [10.1103/PhysRevA.101.013801](https://doi.org/10.1103/PhysRevA.101.013801)**I. INTRODUCTION**

Techniques to characterize quantum states have become more and more valuable with the development of quantum information science. In order to establish standards and check the compliance of the different building blocks, it is necessary to have efficient and reliable measurement methods. However, characterizing quantum states is challenging by nature [1]. One quantum measurement only provides a limited amount of information and therefore it is always necessary to perform multiple measurements to obtain a full quantum state characterization. All the art lies in the way of assembling those pieces of information [2,3].

Beyond the conceptual interest, it is also important to pay attention to the practical aspects: Each measurement demands experimental resources, e.g., time, energy, money, and processing power. Regarding the valuable character of the measurements, it is thus essential to know how the choice of the experimental parameters, on one hand, and the evaluation technique, on the other hand, can maximize the amount of extracted information. In other words, the question is how to obtain the desired characterization at reduced *costs*.

Optical states constitute the essential ingredient of many quantum information protocols, for quantum-network applications [4,5] as well as all-optical processing [6]. Among the different degrees of freedom that define an optical mode, the temporal shape has lately attracted increasing interest [7]. However, it appears to be challenging to control [8]. Although theoretical models have been developed for various systems [9,10], they don't always accurately describe the experimental implementation. Hence, in order to verify, experimental techniques to measure the temporal mode are necessary. The Hong-Ou-Mandel experiment was probably the first technique looking closely at the characterization problem of temporal modes [11]. Although it gives information about the coherence of the temporal shape, this technique evaluates the degree of indistinguishability and does not provide any information about the details of a possible mismatch. In addition, it remains restricted to single-photon states.

Recently new methods have been developed to tackle the challenge in practical cases [12–18]. Those techniques are

mostly based on homodyne detection. With some analogies with the methods developed for the spatial degree of freedom [19], recent techniques have shown that the use of the autocorrelation function from homodyne measurements is an efficient strategy. However, in the technique presented in Ref. [14], only real-valued temporal mode functions can be reconstructed. Reference [12] proposed a solution to reconstruct temporal mode functions with complex values by performing measurements at various detunings of the local oscillator. Those additional measurements require a sophisticated algorithm in order to extract the temporal density matrix. Another procedure has been proposed in [15]. There, one frequency is sufficient but then the use of a double homodyne detection is required.

Following those works, here we provide new insights regarding the problem of experimental costs we just underlined. Starting from reasonable assumptions, we propose an alternative to extract the complex-valued temporal mode function without the need of additional measurements nor increasing the complexity of the data processing or experimental apparatus. In addition, we also address the question of the accuracy of the results and evaluate the conditions under which a maximum of valuable information can be extracted. Therefore, we provide here a turnkey method that can be successfully used in a wide range of systems beyond the usual continuous-variables framework.

II. TEMPORAL MODE RECONSTRUCTION

The reconstruction procedure is depicted in Fig. 1. The signal recorded by a continuous wave (cw) homodyne detection is a time-dependent measurement of the quadrature observable $\hat{x}_\theta(t)$. Here, θ represents the phase between the local oscillator and the measured state. In the following, we assume that all the recordings are done with phase averaging (see Appendix B) and thus omit the notation in the following. From those quadrature signals we compute the autocorrelation function $\langle \hat{x}(t)\hat{x}(t') \rangle$ which can be represented as $K(t, t')\sigma_0^2$. The associated kernel K is independent of the variance of the vacuum $\sigma_0^2 = \langle 0|\hat{x}^2|0 \rangle$.

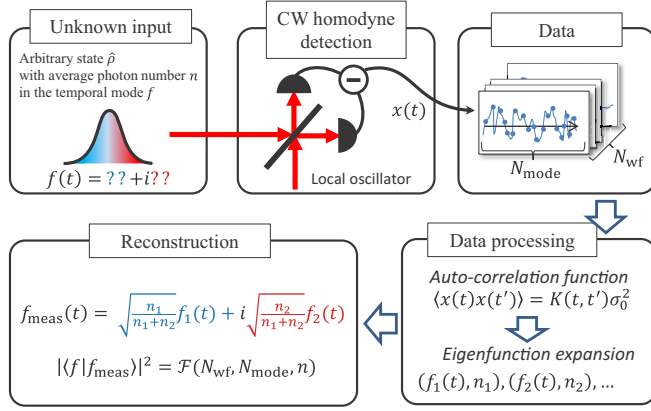


FIG. 1. Principle of the temporal mode reconstruction. The state with an unknown complex-valued temporal shape f is measured by a continuous wave (cw) homodyne detection. The collected data are used to compute the autocorrelation function. Then, by applying the eigenfunction expansion, we use two of the eigenfunctions and associated eigenvalues to reconstruct the temporal mode f_{meas} . Knowing the average photon number n , the accuracy of the reconstruction, given by the fidelity \mathcal{F} between f and f_{meas} , can be set by the choice of the number of waveforms N_{wfr} and the number of measured modes N_{mode} .

Assuming the measurement of an arbitrary state in a pure single temporal mode defined by the function f , e.g., a single-photon state $\hat{a}_f^\dagger|0\rangle = \int dt f(t)\hat{a}^\dagger|0\rangle$, the kernel is of the form,

$$K(t, t') = \delta(t - t') + 2\langle \hat{n}_f \rangle \text{Re}[f(t)f^*(t')], \quad (1)$$

where $\langle \hat{n}_f \rangle$ is the average photon number (see Appendixes). As shown in [14], if f is real, one can immediately identify that it is also an eigenfunction of the kernel K with the associated eigenvalue $\kappa = 2n_f + 1$. Any other function orthogonal to f is an eigenfunction, too, but with an eigenvalue equal to 1. Hence, by measuring K , the function f will correspond to the eigenfunction associated with the largest eigenvalue, i.e., $\kappa > 1$.

If f is a function with complex values, we have to consider more than one eigenfunction. Indeed, the second term of Eq. (1) can be expanded in the following way:

$$\text{Re}[f(t)f^*(t')] = \text{Re}[f(t)]\text{Re}[f^*(t')] + \text{Im}[f(t)]\text{Im}[f^*(t')]. \quad (2)$$

Hence, we recognize the eigenfunction expansion which is always guaranteed by Mercer's theorem [20] since $K(t, t')$ is symmetric positive. If we call ϕ the argument of the function f such that $f(t) = |f(t)|e^{i\phi(t)}$, we have the two eigenfunctions of K :

$$f_1(t) = \sqrt{\frac{n_1+n_2}{n_1}}|f(t)|\cos(\phi(t) + \phi_0), \quad (3)$$

$$f_2(t) = \sqrt{\frac{n_1+n_2}{n_2}}|f(t)|\sin(\phi(t) + \phi_0). \quad (4)$$

Those two eigenfunctions are associated with the eigenvalues $\kappa_i = 2n_i + 1$ with n_i being the average photon number in the mode f_i . The energy conservation is satisfied by $\langle \hat{n}_f \rangle = n_1 + n_2$. Note that ϕ can be redefined up to any arbitrary global

phase, and here, ϕ_0 only ensures the orthogonality for a given $\phi(t)$, i.e., $\int f_1(t)f_2(t)dt = 0$. As for the case of f being real, all the other eigenfunctions, being orthogonal to f_1 and f_2 , are associated to the eigenvalues equal to 1, thus corresponding to the vacuum states. Eventually, the temporal mode function is reconstructed with the two eigenfunctions and their associated average photon numbers,

$$f(t) = \frac{1}{\sqrt{n_1 + n_2}}(\sqrt{n_1}f_1(t) + i\sqrt{n_2}f_2(t)). \quad (5)$$

However, with only one frequency for the local oscillator, an ambiguity on the sign of the phase remains. Indeed, without prior knowledge about f , there is no way to discriminate which eigenfunction is f_1 and which one is f_2 . In other words, which eigenfunction has to be taken as the real part and which one is the imaginary part of f . This is analog to the case of the beating signal of two waves: Only the absolute difference of frequencies is measured and it is not possible to tell which one of the two waves has the largest frequency. However, as soon as one has a second reference, this ambiguity can be lifted. Eventually, in practice, it is not unusual that one has some knowledge about the characterized photonic state and, depending on the tested physical system, one can maybe infer information about which sign makes sense.

III. MULTIMODE AND STATISTICAL MIXTURE

As mentioned previously, to apply the proposed reconstruction we need to assume that the measured state lies in a pure single temporal mode. (Note that here the purity concerns the mode but that the state within the mode can be a statistical mixture though.) However, this assumption can be checked *a posteriori*.

Three cases are possible. First, if only one eigenvalue is greater than one, there is no ambiguity; the state is in a pure real-valued temporal mode. Second, if more than two eigenvalues are greater than one, then there are more than two modes involved. What can be said about the details of these modes is beyond the scope of this paper and probably requires some assumptions. For example, in Refs. [14,16] all temporal modes are assumed to be pure and with real values. Third, if two eigenvalues are above one, either there is a pure complex-valued temporal mode, or there are two modes (mixed or pure). Nevertheless, the pure single-mode case can be confirmed by performing a new reconstruction with the compensating phase $\phi(t)$ on the local oscillator, effectively making f real valued. This way, the new reconstruction should exhibit only one eigenvalue above one. If not, then we can conclude that the mode was not pure and/or single.

IV. RECONSTRUCTION ACCURACY

For any reconstruction method it is important to be able to evaluate its accuracy. For nontrivial cases like here, the usual approach consists in performing multiple simulations: Given some results, one can estimate the uncertainty and therefore how close these results are from the real state. However, the accuracy is known only *a posteriori*. Considering the *experimental costs* of the measurements, it can be valuable to know in advance how accurate the reconstruction can be.

Practically, the implementation of the method requires some unavoidable parameter choices. In our reconstruction method, three parameters have to be considered:

- (1) N_{wf} , the number of waveforms acquired from the homodyne signal.
- (2) N_{mode} , the number of modes which are measured.
- (3) $\langle \hat{n}_i \rangle$, the average photon number per mode i .

First, the number of measured waveforms used to compute the kernel $K(t, t')$ is finite which will obviously lead to some statistical limitations.

Second, each waveform will be recorded at a finite rate and for a finite duration. Ideally, the number of samples per waveform N_{samp} simply corresponds to the number of modes. If we try to get a description closer to the experimental implementation, one has to consider the different electronic stages from the photodiodes to the analog-to-digital converter which define an overall limited bandwidth. Therefore, the different modes are not measured with the same gain. Hence, the effective number of measured modes is in this case given by $N_{\text{mode}} \propto \Delta\omega/\delta\omega$, namely the ratio of the bandwidth by the resolution bandwidth. The case $N_{\text{mode}} = N_{\text{samp}}$ is then only true if the bandwidth is larger than the sampling frequency $1/\delta t$.

Eventually, the average photon number $\langle \hat{n} \rangle$ is not strictly speaking an experimental parameter as it cannot be adjusted. Nevertheless, improving the efficiency of a homodyne detection can be challenging and therefore it is valuable information to know how rewarding the improvement of the efficiency of the setup would be.

In order to quantify the impacts of those parameters on the results, we have performed multiple Monte Carlo simulations and compared input (f, n) and output $(f_{\text{meas}}, n_{\text{meas}})$. From this we infer the dependency between the results accuracy and the different parameters. We do not make any mathematical proof and therefore the conclusion we provide should be considered as a help for performing measurements. Most of the raw simulation results are reported in Appendix D.

The similarity between f and f_{meas} is usually quantified by the fidelity $\mathcal{F} = |\int dt f^*(t)f_{\text{meas}}(t)|^2$. Here, as the fidelity will be ideally close to unity, we analyze the infidelity $\delta\mathcal{F} = 1 - \mathcal{F}$. Concerning the evaluation of the photon number, we look at the deviation defined by $\delta n = n_{\text{meas}} - n$. As shown by Eq. (5), when f has complex values, the reconstruction requires one to combine two eigenmodes. For simplicity, we first focus on the reconstruction involving one eigenmode. This corresponds to the case of f being real, in which case we label the fidelity $\mathcal{F}_{\mathbb{R}}$. This case also applies to complex-valued functions when looking at the real or imaginary part individually.

Hence, over multiple simulations, we have found that the average value of the infidelity has the form,

$$\mu(\delta\mathcal{F}_{\mathbb{R}}) \approx \frac{N_{\text{mode}}/2}{N_{\text{wf}}} \times \frac{1}{n} \left(1 + \frac{1}{2n}\right), \quad (6)$$

and a standard deviation,

$$\sigma(\delta\mathcal{F}_{\mathbb{R}}) \approx \frac{\sqrt{N_{\text{mode}}/2}}{N_{\text{wf}}} \times \frac{1}{n} \left(1 + \frac{1}{2n}\right). \quad (7)$$

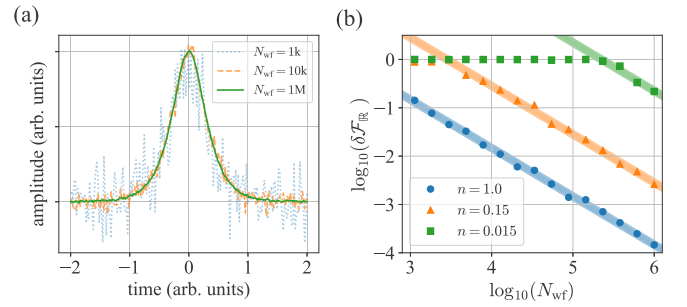


FIG. 2. (a) Temporal shape for different values of N_{wf} . (b) Infidelity versus N_{wf} for different values of the average photon number n . The filled areas correspond to the 2σ distributions, i.e., $\mu(\delta\mathcal{F}) \pm 2\sigma(\delta\mathcal{F})$. For (a) and (b) $N_{\text{mode}} = N_{\text{samp}} = 200$.

Figure 2(a) shows the outcome of the temporal mode function reconstruction f_{meas} for the simulation of a real function f (with $n = 1$ and $N_{\text{mode}} = N_{\text{samp}} = 200$). We can see that even with a small number of waveforms the shape can already be observed. However, the noise decreases with increasing N_{wf} .

Interestingly, Fig. 2(b) shows that there is a clear threshold when $\mu(\delta\mathcal{F}) = 1$ which basically means that no f_{meas} can be reconstructed or in other words, f_{meas} has no overlap with f . Hence, with an *a priori* coarse knowledge of n , the choice of the parameters should fulfill the condition $\sqrt{\frac{N_{\text{mode}}}{N_{\text{wf}}}} \ll n$.

Another important message here is that a too large number of modes is detrimental for the accuracy. This is actually counterintuitive as it means that an excessively large electronic bandwidth (or a too high time resolution) and/or a too small frequency resolution (or too long waveform duration) reduces the achievable accuracy.

Conversely, N_{mode} cannot be too small either as with an undersampling the details of the shape would be missing. Here, this is not caught by the simulations. Indeed, a continuous function and a discretized function don't have a unity overlap but here we compute the fidelity between f and f_{meas} both being sampled the same way. Although that is a trivial problem, it is really specific to each temporal mode shape and therefore not possible to study in the most general case. In other words, in relation to the Nyquist-Shannon theorem, this defines a lower bound on N_{mode} .

As shown by Eq. (5), the average photon numbers obtained from the eigenvalues are part of the reconstruction when considering a complex-valued temporal mode function. Therefore, it is important to understand their accuracy, too. In Fig. 3(a), for a vacuum state on every mode, the average photon number for each mode can be above or below zero. This is due to the statistical limitation (but not exclusively as we will see next). Hence, by increasing the number of waveforms N_{wf} , we see that this deviation decreases. We find that on average the deviation follows:

$$\mu(\delta n)_{|0\rangle} \approx \sqrt{\frac{N_{\text{mode}}}{N_{\text{wf}}}}. \quad (8)$$

In Fig. 3(b) we can see that this formula (dashed black line) is also the bound for states different than vacuum. Beyond this

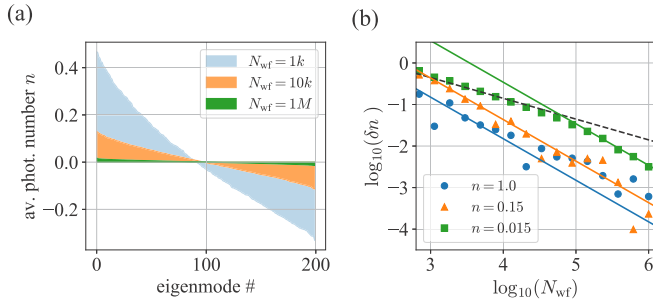


FIG. 3. (a) Average photon number of vacuum states obtained from the eigenfunction expansion for different N_{wf} . Ideally all values should be zero but the statistical limitation given by N_{mode} and N_{wf} leads to a deviation. (b) Scan of N_{wf} for different values of n . The plain line gives $\mu(\delta n)$ from Eq. (9). The dashed line is the upper bound given by the vacuum state $\mu(\delta n)_{|0\rangle} \approx \sqrt{N_{\text{mode}}/N_{\text{wf}}}$.

bound, when $n \neq 0$, the average value of the deviation δn is

$$\mu(\delta n) \approx \frac{N_{\text{mode}}/2}{N_{\text{wf}}} \left(1 + \frac{1}{2n}\right). \quad (9)$$

Therefore, one can only measure modes with photon numbers n by fulfilling the condition $n \gg \sqrt{\frac{N_{\text{mode}}}{N_{\text{wf}}}}$ which is similar to the condition found for the fidelity of the temporal function. This bound is well illustrated in Fig. 3(b) by the case of $n = 0.015$.

The standard deviation for n is not specific to the reconstruction we use here. It is limited by the amount of data even when knowing the temporal mode f or using single photon counting. In addition, it is specific to the photon number distribution of the quantum state. Thus we cannot provide any general formula.

As announced earlier, all the previous results apply to the case of single eigenmodes. Now, knowing how accurate each individual mode is, we are interested in the full reconstruction given by Eq. (5) which involved two eigenmodes. Due to this combination of eigenmodes, the analysis of the accuracy is less straightforward. Indeed, the division of the global average photon number n between n_1 and n_2 is not independent of the temporal mode function f . However, under the condition $n \gg \sqrt{\frac{N_{\text{mode}}}{N_{\text{wf}}}}$, we can distinguish two extreme cases: First, when the temporal mode function is real and second, when it is complex with balanced contributions on the real and imaginary parts.

When the temporal mode function f is real but no *a priori* assumption can be made, the contribution of the second mode necessarily degrades the fidelity. This contribution essentially comes from the nonzero photon number measured for the second mode. As shown earlier, even the vacuum state shows a deviation in the photon number $\mu(\delta n)_{|0\rangle}$. Hence, the fidelity will be bounded by $\mu(\delta n)_{|0\rangle}/n$. In this case the scaling is less favorable compared to the reconstruction when assuming a real function. A possible strategy to improve the accuracy would be to split the data set into two in order to minimize the error on n_2 .

The second extreme case is when the complex-valued function f leads to a balanced division of the average photon number, i.e., $n_1 = n_2$. In that case, the average fidelity is straightforward to calculate and is equal to the one in Eq. (6) but the average photon number has to be replaced by $n/2$.

In summary, without any assumption on f and more precisely on the photon number division n_1 and n_2 , but assuming that $n \gg \sqrt{\frac{N_{\text{mode}}}{N_{\text{wf}}}}$ is fulfilled, the fidelity of the reconstructed state will be bounded by those two aforementioned cases:

$$\frac{N_{\text{mode}}/2}{N_{\text{wf}}} \frac{1}{n/2} \left(1 + \frac{1}{n}\right) \lesssim \mu(\delta \mathcal{F}_{\mathcal{C}}) \lesssim \frac{1}{n} \sqrt{\frac{N_{\text{mode}}}{N_{\text{wf}}}}. \quad (10)$$

In practice, the choice of parameters can be done in the following way. One starts with the minimal discretization of f that is acceptable, which defines N_{mode} . Then, with a prior estimate of the average photon number n , one calculates the N_{wf} that will give the desired accuracy. If N_{wf} is too large, then one can consider improving the detection efficiency and therefore increasing n . If N_{wf} is not too large, then one has some room in the choice of N_{mode} and the level of accuracy.

V. EXPERIMENTAL ILLUSTRATION

In the following we check our method experimentally. As mentioned in the introduction, we restrict our study to the impact of statistical limitations. The effect of experimental imperfections is a relevant topic, too, but cannot be modeled in a general way. However, we assume that our system is good enough and we show how the various conclusions we have drawn are applicable and thus fruitful practically.

We illustrate our method with a temporal mode with the shape “MPQ” in the polar representation. This shape has the advantage of probing the technique with a relatively sophisticated shape in amplitude and phase. The duration and dynamics of the shape are chosen to be within the band of the homodyne detection (band pass of 10 kHz to 3 MHz). The probe state is a coherent state obtained via a weak cw laser beam sent through an acousto-optic modulator (AOM) such that the desired shape is imprinted on the beam. Details about the experimental setup can be found in Appendix A.

Figure 4 shows the experimental results. On the histogram [Fig. 4(a)] we see the two relevant eigenvalues for the reconstruction. We also show in the inset the spectrum of the vacuum state. This later allows us to estimate the number of modes measured by the homodyne detection and therefore estimate the accuracy of the reconstruction. The plot [Fig. 4(b)] depicts the two eigenfunctions associated with the two eigenvalues significantly above 1. The plain lines represent the measured functions whereas the dotted lines represent the theoretical ones. In Fig. 4(c) we plot those two functions in a parametric way which corresponds to the polar representation of the complex-valued temporal mode.

Eventually, we check how the fidelity changes by repeating the same reconstruction for different average photon numbers and various numbers of waveforms. In Fig. 4(d), we show $\delta \mathcal{F}$ as a function of the number of waveforms N_{wf} . The two bounds described in Eq. (10), namely the balanced and unbalanced mode distributions, give a satisfying range of accuracy for the reconstructed temporal functions. One can see, however, that the fidelity settles for high N_{wf} . We attribute this to the experimental precision of the generation of the probe state, one possible issue being the calibration of the nonlinear response of the acousto-optic modulator. Furthermore, we cannot exclude, regardless of the source, some phase and/or

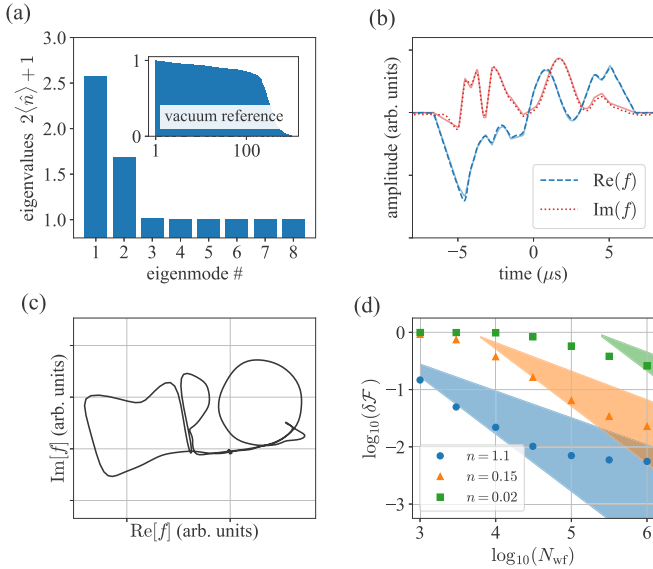


FIG. 4. Experimental demonstration. (a) Spectrum of eigenvalues. The inset is the spectrum measured for the vacuum state input that is used to determine the relevant number of modes measured by the homodyne detection. (b) Eigenfunctions that correspond to the real and imaginary part of the temporal mode functions. Dashed and dotted lines are the measured functions and the solid lines the targeted ones. (c) Polar plot of the temporal mode function reconstructed via Eq. (5). The fidelity with the target shape “MPQ” is equal to $\mathcal{F} = 99.44\%$. This data set contains $N_{\text{wrf}} = 1\text{M}$ waveforms and the input probe state an average photon number of $n = 1.1$. (d) Infidelity as a function of the number of waveforms N_{wrf} for three values of n . Regarding the inset of (a), we consider $N_{\text{mode}} = 100$. The colored areas correspond to the limits defined by Eq. (10).

amplitude noise. The latter issue should translate into more eigenvalues above 1 but at such a low level that it is difficult to measure those eigenvalues without a tremendous amount of measurements.

It is worth noting that our method is relatively robust to losses. Indeed, whereas the measurement of highly negative Wigner functions or strongly squeezed states of light requires highly efficient homodyne detections [21,22], here, losses translate into a reduction of the average photon number only. Of course, this impacts the demand on the amount of measurement, i.e., the number of waveforms, but does not limit the possible high fidelity of the reconstructed state. Such a feature is particularly important for quantum states of light propagating in a quantum network. For instance, our characterization in Fig. 4(d) with $n = 0.15(0.02)$ would correspond to the losses on a single photon propagating over 40(80) km of fiber.

VI. CONCLUSION

Here, we have provided a full recipe to reliably characterize any arbitrary complex-valued temporal mode function. This method features an extremely simple implementation in terms of the experimental setup as well as data processing. Importantly, we provide all the key aspects that are mandatory to guarantee a trustworthy reconstruction with a reduced amount of resources. This can be a game changer as we have

shown that some aspects can be counterintuitive at first sight. In addition, we have illustrated the method on an experimental case and confirmed that it is a powerful way to reconstruct even a sophisticated shape. Hence, we believe that this will facilitate the implementation of the presented technique beyond the continuous variables community and make this technique a standard routine in quantum optics laboratories [23].

ACKNOWLEDGMENTS

The authors thank S. Dürr for fruitful discussions. This work was supported by the Bundesministerium für Bildung und Forschung via the Verbund Q.Link.X (Grant No. 16KIS0870), by the Deutsche Forschungsgemeinschaft under Germany’s Excellence Strategy, EXC-2111 Grant No. 390814868, and by the European Union’s Horizon 2020 research and innovation programme via the project Quantum Internet Alliance (QIA, Grant Agreement No. 820445).

APPENDIX A: EXPERIMENTAL FACTS

In this section we provide technical information about our experimental setup. It shows what kind of performances are sufficient to reach a reconstruction fidelity as high as 99.44% shown in Fig. 4.

The light pulse is obtained by an attenuated cw laser beam modulated in amplitude and phase by an AOM (G&H). This AOM is driven by a 14-bit direct digital synthesizer (DDS AD9910). The chip is programed with the desired profile in amplitude and phase. However, it is not directly the temporal mode function f as the AOM has a nonlinear response. This latter can be fitted with a \sin^4 function. Therefore we pre-compensate f in the programed profile.

The homodyne detector is a homemade circuit using a transimpedance architecture (operational amplifier LMH6624, $R_f = 10\text{k}\Omega$). More details on the topic can be found in [24,25]. Working at 780 nm, we use a pair of matched Si photodiodes (Hamamatsu S3883).

The signal is then amplified by 40 dB (Femto HVA-10M-60-B; settings are AC coupled, 40-dB gain) and low pass filtered down to 2.5 MHz (Mini-Circuits BLP-2.5+).

The homodyne detection is characterized with a spectrum analyzer (see Fig. 5). In order to obtain a trustworthy reconstruction, few features should be observed on this spectrum characterization.

(1) A good clearance between the electronic noise and the signal (shot noise). As shown in [26] this essentially translates as an equivalent optical loss. Here, with approximately 17 dB, we have an equivalent efficiency of 98%. Generally speaking, this value can be increased by the feedback resistance of the transimpedance circuit but at the expense of a reduction of the bandwidth. Alternatively, the power of the local oscillator can be increased but at the risk to either saturate the semiconductor [27] or even reach the damage threshold.

(2) An efficient rejection of the classical noise present on the local oscillator. This is achieved by a good balancing of the light power on the two photodiodes. Our laser source (DL Pro, Toptica) essentially shows noise below a few hundred kHz. Here the shot noise spectrum clearly shows a good cancellation of this noise.

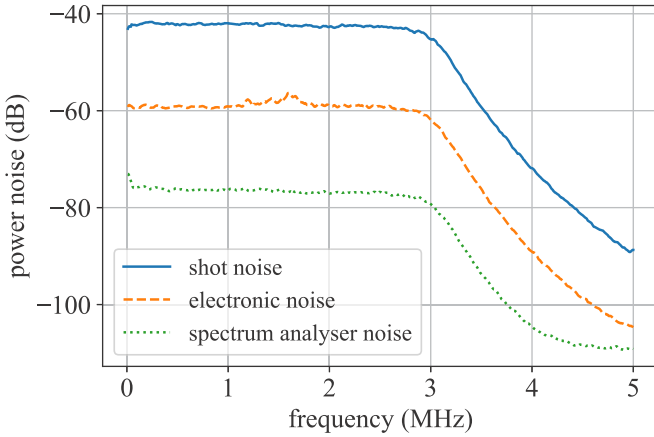


FIG. 5. Homodyne signal analysis. The local oscillator power is 2 mW (1 mW per photodiode).

(3) A flat response over the frequency range of interest. Although we did not do it for our measurements, this can be corrected by postprocessing on the recorded data.

Ultimately, the homodyne signal is recorded by a 12-bit oscilloscope (Lecroy Wave Runner HRO 66Zi). Note that here the 12-bit accuracy does not provide any advantage. Indeed, our electronic signal-noise clearance of approximately 17 dB is the main limitation, an 8-bit resolution would limit the signal-to-noise ratio to 24 dB.

The optical efficiency is usually an important figure of merit but for our method there is no strict limit. Practically, a high efficiency reduces the constraint on the choice of N_{wf} and N_{mode} . For our setup, we reached 75% with standard optical components [23]. However, the average photon numbers given in Fig. 4 are not compensated for this efficiency value.

APPENDIX B: GENERALIZATION TO ANY STATE IN A SINGLE MODE

We show in the following one possible way to derive Eq. (1) of the main text. (The proof is relatively straightforward in the case of a single-photon state). The autocorrelation function of the quadrature operators can be expressed as a function of the annihilation and creation operators:

$$\begin{aligned}\hat{x}_\theta(t)\hat{x}_\theta(t') &= (e^{-i\theta}\hat{a}(t) + e^{i\theta}\hat{a}^\dagger(t))(e^{-i\theta}\hat{a}(t') + e^{i\theta}\hat{a}^\dagger(t')) \\ &= e^{-2i\theta}\hat{a}(t)\hat{a}(t') + e^{2i\theta}\hat{a}^\dagger(t)\hat{a}^\dagger(t') \\ &\quad + (\hat{a}(t)\hat{a}^\dagger(t') + \hat{a}^\dagger(t)\hat{a}(t')).\end{aligned}\quad (\text{B1})$$

First, due to the phase averaging,

$$\hat{x}(t)\hat{x}(t') = \frac{1}{2\pi} \int_{[0, 2\pi]} \hat{x}_\theta(t)\hat{x}_\theta(t') d\theta, \quad (\text{B2})$$

the first two terms vanish. Second, by using the commutation relation $[\hat{a}(t), \hat{a}^\dagger(t')] = \delta(t - t')$ we obtain

$$\hat{x}(t)\hat{x}(t') = \delta(t - t') + \hat{a}^\dagger(t')\hat{a}(t) + \hat{a}^\dagger(t)\hat{a}(t'). \quad (\text{B3})$$

We call f the temporal mode in which the measured state $\hat{\rho}$ lies. Hence, we can define a set of orthonormal functions $\{f_k\}$ with $f = f_{k_0}$. With this set of functions forming a complete

basis, we have $\hat{a}(t) = \sum_k f_k(t)\hat{a}_k$. Hence, we can write

$$\hat{a}^\dagger(t)\hat{a}(t') = \sum_k \sum_{k'} f_k^*(t)f_{k'}(t')\hat{a}_k^\dagger\hat{a}_{k'}. \quad (\text{B4})$$

As we assume a single-mode state, all other temporal modes $f_{k \neq k_0}$ contain the vacuum state. Therefore, we have $\langle \hat{a}_{k_0}^\dagger \hat{a}_{k_0} \rangle = \langle \hat{n}_f \rangle$ and, for any $k \neq k_0$ or $k' \neq k_0$, we have $\langle \hat{a}_k^\dagger \hat{a}_{k'} \rangle = 0$. The average of Eq. (B3) becomes

$$\langle \hat{x}(t)\hat{x}(t') \rangle = \delta(t - t') + \langle \hat{n}_f \rangle [f^*(t)f(t') + f^*(t')f(t)] \quad (\text{B5})$$

$$= \delta(t - t') + 2\langle \hat{n}_f \rangle \text{Re}[f^*(t)f(t')]. \quad (\text{B6})$$

It is important to note that no assumptions are made on the input state beside the fact that it lies in a pure single temporal mode. This proves that the reconstruction of the temporal mode function is independent of the state $\hat{\rho}$ and that only the average photon number plays a role in the reconstruction. One can measure the temporal mode function regardless of the state within that mode (Fock states, coherent states, squeezed vacuum, etc.).

APPENDIX C: HOMODYNE SIGNAL SIMULATION

The signal $x(t)$ is actually discrete such that $x(t_i) = x_i$ and limited in duration such that $i \in [0, N_{mode} - 1]$. For each homodyne signal and for each mode f_k we need to generate N_{mode} random values x_k . In the case of a temporal mode function with real values only, only one mode can potentially contain one photon, all the others being the vacuum state. Thus, we need one random number x_0 following the single-photon distribution $\mathcal{P}_{|1\rangle}(x)$ and all the others $x_{k \neq 0}$ following the vacuum distribution $\mathcal{P}_{|0\rangle}$ (Gaussian distribution). From this set, and by defining f_0 the mode of the single-photon state, one can compute the homodyne signal,

$$x(t_k) = \sum_{j=1}^{N_{mode}} x_j f_j(t_k). \quad (\text{C1})$$

It is then possible to apply at this stage low- and/or high-pass filters. However, it is safer to then start with a longer time segment and truncate it after the filtering in order to minimize edge effects.

The case of a temporal mode with complex values is more tricky. First one needs to split the temporal function into real and imaginary part. One obtains

$$\int f(t)\hat{a}^\dagger(t)dt|0\rangle = \int [t f_r(t) + i r f_i(t)]\hat{a}^\dagger(t)dt|0\rangle \quad (\text{C2})$$

$$= [t\hat{a}_r^\dagger + i r\hat{a}_i^\dagger]|0\rangle, \quad (\text{C3})$$

where $r^2 + t^2 = 1$. We thus have a conditional probability between the two modes such that the probability to measure x_r in the real mode and x_i in the imaginary mode is

$$\begin{aligned}\mathcal{P}_{r,i}(x_r, x_i) &= \eta |\langle x_r | \langle x_i | [t\hat{a}_r^\dagger + r\hat{a}_i^\dagger]|0\rangle|^2 \\ &\quad + (1 - \eta) |\langle x_r | \langle x_i | |0\rangle|^2 \\ &= \eta (t^2 \mathcal{P}_{|1\rangle}(x_r) \mathcal{P}_{|0\rangle}(x_i) + r^2 \mathcal{P}_{|0\rangle}(x_r) \mathcal{P}_{|1\rangle}(x_i)) \\ &\quad + (1 - \eta) \mathcal{P}_{|0\rangle}(x_r) \mathcal{P}_{|0\rangle}(x_i).\end{aligned}\quad (\text{C4})$$

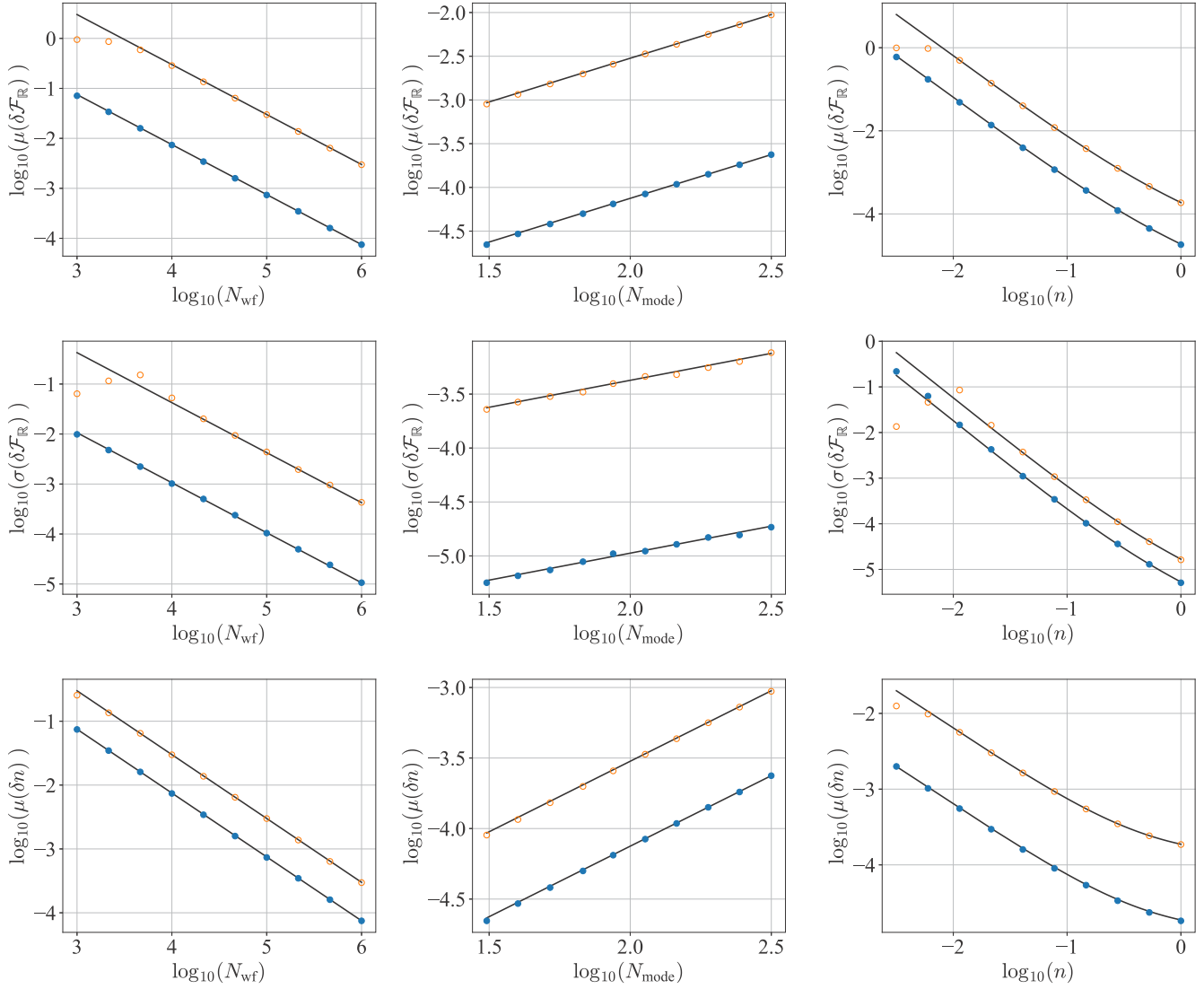


FIG. 6. Simulation with reconstruction assuming a real-valued temporal mode function. (First column) Scans of the parameter N_{wf} , plain circles for the parameters $N_{mode} = 100$ and $n = 1.0$, open circles for $N_{mode} = 100$ and $n = 0.1$. (Second column) Scans of the parameter N_{mode} , plain circles for the parameters $N_{wf} = 1$ M and $n = 1.0$, open circles for $N_{wf} = 1$ M and $n = 0.1$. (Third column) Scans of the parameter n , plain circles for the parameters $N_{mode} = 25$ and $N_{wf} = 1$ M, open circles for $N_{mode} = 250$ and $N_{wf} = 1$ M. All scans show very good agreement between deduced formulas and simulations.

Practically, this results in generating x_r with the distribution,

$$\mathcal{P}_r(x_r) = \eta(t^2\mathcal{P}_{|1\rangle}(x_r) + r^2\mathcal{P}_{|0\rangle}(x_r) + (1 - \eta)\mathcal{P}_{|0\rangle}(x_r), \tag{C5}$$

and then, for the given x_r , one generates x_i following the distribution $\mathcal{P}_{r,i}(x_r, x_i)$.

Regarding the temporal mode analysis process, the correlation is in principle unimportant and random numbers could be chosen independently for the two modes. However, it would be questionable to apply this assumption here as we want to check that the procedure is giving the expected results.

We have also performed simulations for coherent states. These simulations do not present this problem of correlated modes. Indeed, by essence a coherent state doesn't lead to entanglement via linear operations. On the other hand, in contrast to the single-photon state, a coherent state has a

phase. Hence, in that case one needs a proper phase averaging implementation.

APPENDIX D: PARAMETER ESTIMATION

In order to infer the formulas describing the accuracy of the estimation of f_{meas} and n_{meas} , we have realized various sets of simulation where we scan the value of the main three parameters N_{wf} , N_{mode} , and n .

Figure 6 shows some of the simulation results used to infer the formulas exposed in the main text. The plain black lines are not fits but the corresponding equations are given in the main text. For each case we use two sets of parameters to show that the variables are independent.

Figure 7 corresponds to the simulation in the case of complex-valued function reconstructions for a real function

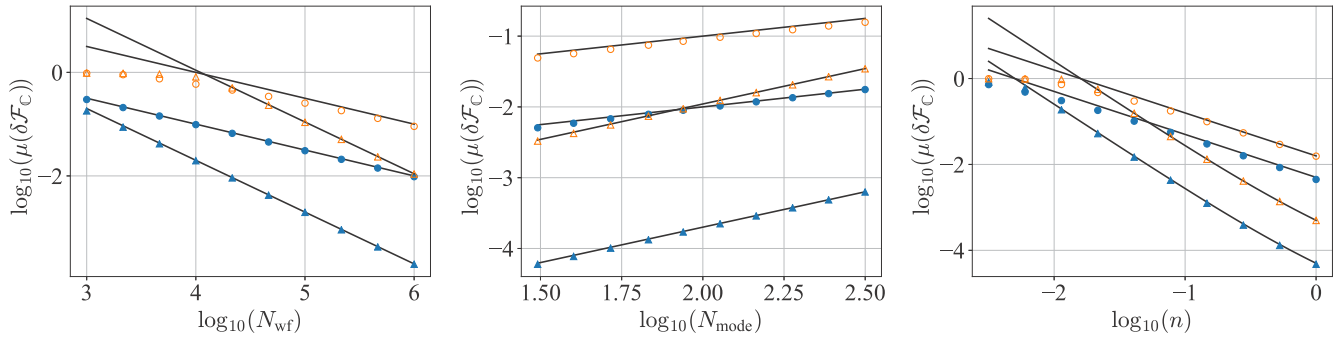


FIG. 7. Comparison of a complex-valued reconstruction for a real temporal function (circle) and a complex-valued function with balanced photon numbers (triangle). (Left graph) Scans of the parameter N_{wf} , plain markers for the parameters $N_{\text{mode}} = 100$ and $n = 1.0$, open markers for $N_{\text{mode}} = 100$ and $n = 0.1$. (Middle graph) Scans of the parameter N_{mode} , plain markers for the parameters $N_{\text{wf}} = 1 \text{ M}$ and $n = 1.0$, open markers for $N_{\text{wf}} = 1 \text{ M}$ and $n = 0.1$. (Right graph) scans of the parameter n , plain markers for the parameters $N_{\text{mode}} = 25$ and $N_{\text{wf}} = 1 \text{ M}$, open markers for $N_{\text{mode}} = 250$ and $N_{\text{wf}} = 1 \text{ M}$. All scans show very good agreement between deduced formulas and simulations.

and complex function with balanced eigenvalues (discussion in the main text).

The simulations were performed over the following ranges:

$$\begin{aligned} N_{\text{wf}} &\text{ over } 10^2\text{--}10^7, \\ N_{\text{mode}} &\text{ over } 20\text{--}500, \\ n &\text{ over } 10^{-3}\text{--}10^2. \end{aligned}$$

Therefore, we are confident that the inferred formulas are reliable at least over these ranges.

Running simulations beyond those ranges leads to multiple difficulties: computation time, memory capacity, numerical accuracy, and random number generator cycles. However, a large majority of practical implementations are already covered by the investigated parameter ranges.

- [1] W. K. Wootters and W. H. Zurek, A single quantum cannot be cloned, *Nature (London)* **299**, 802 (1982).
- [2] U. Leonhardt, *Measuring the Quantum State of Light* (Cambridge University Press, Cambridge, 1997).
- [3] C. W. Helstrom, *Quantum Detection and Estimation Theory*, Vol. 123 (Academic Press, Cambridge, 1976).
- [4] H. J. Kimble, The quantum internet, *Nature (London)* **453**, 1023 (2008).
- [5] S. Wehner, D. Elkouss, and R. Hanson, Quantum internet: A vision for the road ahead, *Science* **362**, eaam9288 (2018).
- [6] P. Minzioni *et al.*, Roadmap on all-optical processing, *J. Opt.* **21**, 063001 (2019).
- [7] B. Brecht, Dileep V. Reddy, C. Silberhorn, and M. G. Raymer, Photon Temporal Modes: A Complete Framework for Quantum Information Science, *Physical Review X* **5**, 041017 (2015); **6**, 19901(E) (2016).
- [8] A. I. Lvovsky and M. G. Raymer, Continuous-variable optical quantum-state tomography, *Rev. Mod. Phys.* **81**, 299 (2009).
- [9] A. V. Gorshkov, A. André, M. Fleischhauer, A. S. Sørensen, and M. D. Lukin, Universal Approach to Optimal Photon Storage in Atomic Media, *Phys. Rev. Lett.* **98**, 123601 (2007).
- [10] A. E. B. Nielsen and K. Mølmer, Single-photon-state generation from a continuous-wave nondegenerate optical parametric oscillator, *Phys. Rev. A* **75**, 023806 (2007).
- [11] C. K. Hong, Z. Y. Ou, and L. Mandel, Measurement of Subpicosecond Time Intervals Between Two Photons by Interference, *Phys. Rev. Lett.* **59**, 2044 (1987).
- [12] Z. Qin, A. S. Prasad, T. Brannan, A. MacRae, A. Lezama, and A. I. Lvovsky, Complete temporal characterization of a single photon, *Light: Sci. Appl.* **4**, e298 (2015).
- [13] C. Polycarpou, K. N. Cassemiro, G. Venturi, A. Zavatta, and M. Bellini, Adaptive Detection of Arbitrarily Shaped Ultrashort Quantum Light States, *Phys. Rev. Lett.* **109**, 053602 (2012).
- [14] O. Morin, C. Fabre, and J. Laurat, Experimentally Accessing the Optimal Temporal Mode of Traveling Quantum Light States, *Phys. Rev. Lett.* **111**, 213602 (2013).
- [15] K. Takase, M. Okada, T. Serikawa, S. Takeda, J. Yoshikawa, and A. Furusawa, Complete temporal mode characterization of non-Gaussian states by a dual homodyne measurement, *Phys. Rev. A* **99**, 033832 (2019).
- [16] K. Huang, H. Le Jeannic, V. B. Verma, M. D. Shaw, F. Marsili, S. W. Nam, E. Wu, H. Zeng, O. Morin, and J. Laurat, Experimental quantum state engineering with time-separated heraldings from a continuous-wave light source: A temporal-mode analysis, *Phys. Rev. A* **93**, 013838 (2016).
- [17] C. Baune, J. Fiurášek, and R. Schnabel, Negative Wigner function at telecommunication wavelength from homodyne detection, *Phys. Rev. A* **95**, 061802(R) (2017).
- [18] C. Yang, Z. Gu, P. Chen, Z. Qin, J. F. Chen, and W. Zhang, Tomography of the Temporal-Spectral State of Subnatural-Linewidth Single Photons from Atomic Ensembles, *Phys. Rev. Appl.* **10**, 054011 (2018).
- [19] A. M. Dawes, M. Beck, and K. Banaszek, Mode optimization for quantum-state tomography with array detectors, *Phys. Rev. A* **67**, 032102 (2003).
- [20] R. Courant and D. Hilbert, *Methods of Mathematical Physics*, Vol. 1 (Interscience, New York, 1937).
- [21] O. Morin, V. D'Auria, C. Fabre, and J. Laurat, High-fidelity single-photon source based on a Type II optical parametric oscillator, *Opt. Lett.* **37**, 3738 (2012).

- [22] H. Vahlbruch, M. Mehmet, K. Danzmann, and R. Schnabel, Detection of 15 dB Squeezed States of Light and their Application for the Absolute Calibration of Photoelectric Quantum Efficiency, *Phys. Rev. Lett.* **117**, 110801 (2016).
- [23] O. Morin, M. Körber, S. Langenfeld, and G. Rempe, Deterministic Shaping and Reshaping of Single-Photon Temporal Wave Functions, *Phys. Rev. Lett.* **123**, 133602 (2019).
- [24] O. Morin, Non-Gaussian states and measurements for quantum information, *Quantum Physics* (Université Pierre et Marie Curie - Paris VI, 2013).
- [25] R. Kumara, E. Barrios, A. MacRae, E. Cairns, E. H. Huntington and A. I. Lvovsky, Versatile wideband balanced detector for quantum optical homodyne tomography, *Opt. Commun.* **285**, 5259 (2012)
- [26] J. Appel, D. Hoffman, E. Figueroa, and A. I. Lvovsky, Electronic noise in optical homodyne tomography, *Phys. Rev. A* **75**, 035802 (2007).
- [27] T. Serikawa and A. Furusawa, Excess Loss in Homodyne Detection Originating from Distributed Photocarrier Generation in Photodiodes, *Phys. Rev. Appl.* **10**, 064016 (2018).